ACS Energy LETTERS

http://pubs.acs.org/journal/aelccp

LETTER

Exploiting the Lability of Metal Halide Perovskites for Doping Semiconductor Nanocomposites

Mariano Calcabrini, Aziz Genç, Yu Liu, Tobias Kleinhanns, Seungho Lee, Dmitry N. Dirin, Quinten A. Akkerman, Maksym V. Kovalenko, Jordi Arbiol, and Maria Ibáñez*

Cite This: *ACS Energy Lett.* 2021, 6, 581−587

Read Online

ACCESS | Metrics & More | Article Recommendations | Supporting Information

ABSTRACT: Cesium lead halides have intrinsically unstable crystal lattices and easily transform within perovskite and nonperovskite structures. In this work, we explore the conversion of the perovskite $CsPbBr_3$ into Cs_4PbBr_6 in the presence of PbS at 450 °C to produce doped nanocrystal-based composites with embedded Cs_4PbBr_6 nanoprecipitates. We show that $PbBr_2$ is extracted from $CsPbBr_3$ and diffuses into the PbS lattice with a consequent increase in the concentration of free charge carriers. This new doping strategy enables the adjustment of the density of charge carriers between 10^{19} and 10^{20} cm^{-3}, and it may serve as a general strategy for doping other nanocrystal-based semiconductors.

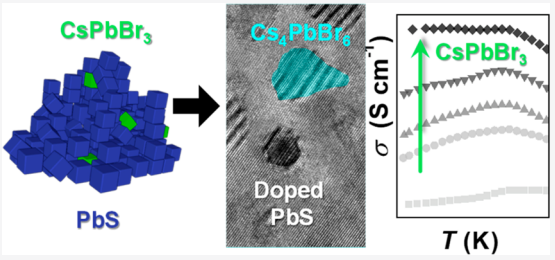

Research on metal halide perovskites is advancing rapidly, owing to the compelling electronic, optical and structural properties of these ionic semiconductors, such as long diffusion lengths and carrier lifetimes,[1−3] low exciton binding energies,[4] low number of trap states despite the high concentration of vacancies,[1,5] composition-tunable bandgap,[6,7] and ease of processability.[8−11] Because of the relatively labile crystal structure of metal halide perovskites, the understanding and control of the chemical and structural transformations that these compounds readily undergo are some of the most pressing questions.[12]

Cesium lead halides can adopt perovskite and nonperovskite structures with different dimensionalities. Perovskites are composed of Cs^+ cations stabilizing $[PbX_6]^{4-}$ octahedra in a cubic or, upon slight distortion, tetragonal or orthorhombic phases, where all the corners of the $[PbX_6]^{4-}$ octahedra are shared.[13] All these compounds adopt regular $CsPbX_3$ stoichiometry (3D). Nonperovskite structures include polymorphs with various stoichiometries, but all of them lose the corner-sharing motif in the lattice. The first example of these structures is a polymorph that despite having the same $CsPbX_3$ stoichiometry crystallizes in an orthorhombic phase (δ-phase) with chains of edge-sharing octahedra (1D).[14] Another example is the lead-depleted Cs_4PbX_6 structure where the $[PbX_6]^{4-}$ octahedra are isolated (0D).[13,15−17] A third closely related nonperovskite structure that has lower Cs^+ content and does not contain $[PbX_6]^{4-}$ octahedra, $CsPb_2X_5$, can be described as layers (2D) of $[Pb_2X_5]^-$ clusters separated by Cs^+ ions.[13,15−17] Because of the large difference in the involved atoms' electronegativities, all these cesium lead halides exhibit mixed bonding nature. The lead halide framework is dominated by covalent bonds and balanced by ionically bound Cs^+ cations. The lack of covalency between Cs^+ and the anionic units enables crystal lability.[18] As a direct consequence, the ions move easily and allow transformation between the different structures—provided that the stoichiometry is compensated.

Very common are the transformations between $CsPbBr_3$ and Cs_4PbBr_6 structures especially in nanocrystals (NCs). The transformation of Cs_4PbBr_6 into $CsPbBr_3$ is achieved by adding $PbBr_2$ to the structure,[19] extracting CsBr by chemical complexation or intercalation,[20] or diffusion and dissolution of CsBr in water.[21] The chemical transformation from $CsPbBr_3$ to Cs_4PbBr_6 can be induced by removing $PbBr_2$ from the crystal lattice by its complexation with thiols or amines.[22−24] In all

Received: November 24, 2020
Accepted: January 11, 2021
Published: January 21, 2021

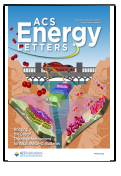

these reactions purification of the NCs is required to separate the undesired byproducts: either CsBr or $PbBr_2$.

PbS NC-based solids find application in various fields including transistors,[25−28] solar cells,[29−32] photodetectors,[31,33,34] and thermoelectrics.[35−37] In most of these applications adjusting the number of free charge carriers to control charge transport is crucial. The conventional n-type dopants for bulk lead chalcogenides are halides. Incorporation of halide ions (X= Cl^-, Br^-, I^-) in the chalcogenide (Y= S^{2-}, Se^{2-}, Te^{2-}) sublattice results in the addition of one electron in the conduction band per halide to compensate for the different valency of halides and chalcogenides.[38] Strategies to dope bulk semiconductors require control over the composition at the impurity level; the straightforward translation into doping bottom-up assembled NC solids is to use doped NCs. However, impurity doping of NCs is energetically[39] and kinetically unfavorable, because the diffusion path of impurity atoms to the surface is short.[40] Although tuning NCs composition has been attempted,[26,41] the introduction of a controlled amount of impurities in small structures is problematic for the preparation of heavily doped semiconductors.[42−44] Alternative approaches to dope NC-based solids have focused on changing the NC surface chemistry,[30,36,38,45−48] inducing partial cation exchange,[49,50] and blending with other NCs.[35,51,52]

PbY−perovskite nanocomposites have been used in photodetectors,[53,54] LEDs,[55,56] and photovoltaics.[57,58] Remarkably, PbS NC inclusions can provide stability to the cubic phase of perovskites suppressing the cubic−orthorhombic phase transition,[59] and perovskite passivation layers enhance charge carrier separation in PbS NCs by providing adequate energy alignment.[60] Furthermore, PbY nanocomposites with secondary phases might be of great importance for thermoelectrics.[35,61]

Herein we propose a strategy to produce doped PbS nanocomposites that makes use of the byproduct of the transformation of $CsPbBr_3$ into Cs_4PbBr_6 and $PbBr_2$, upon heating a mixture of $CsPbBr_3$ and PbS NCs (Scheme 1). Our approach simultaneously introduces dopant ions (Br^-) and a secondary phase (Cs_4PbBr_6) in PbS nanocomposites (Figure 1).

We prepared nanocomposites by mixing PbS NCs with a controlled amount of $CsPbBr_3$ NCs in toluene. This NCs blend was dried under vacuum and annealed with forming gas (5% H_2 in N_2, 1 bar) to yield a powder that was then pressed into pellets with relative densities of ∼92% (Table S1) using spark plasma sintering (Figure 1).

Scheme 1. Chemical Transformation of $CsPbBr_3$ into Cs_4PbBr_6 Triggered by the Dissolution of $PbBr_2$ in PbS

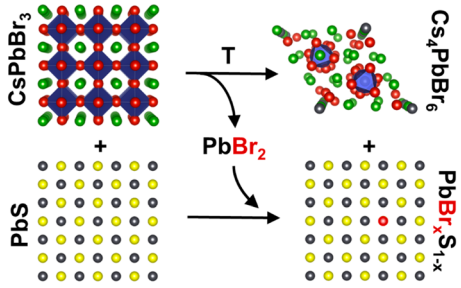

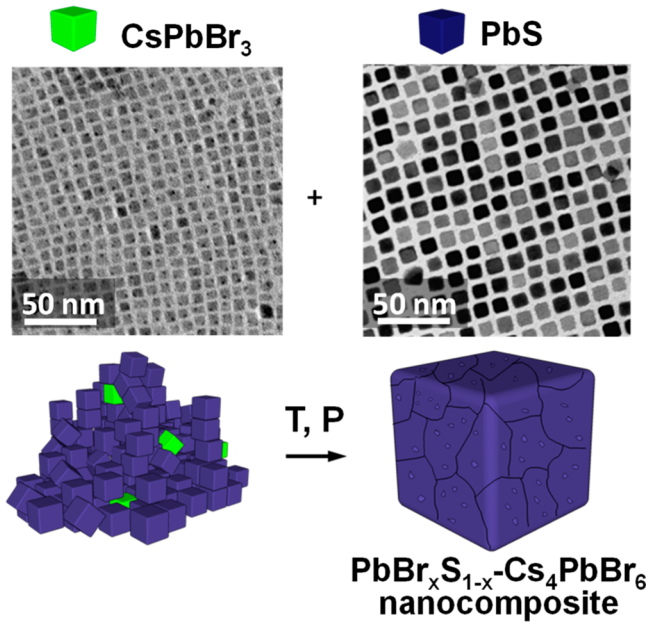

Figure 1. TEM images of the used NCs and scheme of the bottom-up assembly process to produce doped PbS−Cs_4PbBr_6 nanocomposites. The nanocomposites are prepared by blending the NCs in solution, annealing the dried NCs at 450 °C to remove the organic ligands and induce the chemical transformation between $CsPbBr_3$ and Cs_4PbBr_6, and finally pressing the annealed powder at 45 MPa and 500 °C for 5 min to produce the pellets.

To follow the chemical transformation of the perovskites, we performed *in situ* temperature-dependent X-ray diffraction (XRD) measurements of a mixture of PbS NCs and 30% wt. $CsPbBr_3$ NCs (Figures 2 and S1). This mixture was heated to 450 °C and kept at that temperature for 60 min, mimicking the annealing step. Upon heating to 150 °C, $CsPbBr_3$ NCs show strong sharpening of the reflections explained by accelerated ion migration between particles causing grain growth.[62−64] After reaching 450 °C, $CsPbBr_3$ reflections progressively lose intensity, and peaks corresponding to Cs_4PbBr_6 become visible, shifted to lower angles because of thermal expansion of the lattice. This experiment demonstrates that $CsPbBr_3$ converts to Cs_4PbBr_6, necessarily releasing $PbBr_2$. This reaction could be enhanced by the binding affinity of $PbBr_2$ to PbS surface dangling bonds.[65,66] Control experiments with $CsPbBr_3$ and Cs_4PbBr_6 pure phases showed that both phases are recovered after heating to 500 °C and cooling to room temperature and do not undergo any transformation on their own (Figures S9 and S10). Besides, annealing induces crystal grain growth in pure PbS NCs, evidenced by the narrowing of the XRD reflections and scanning electron microscopy (SEM) images (Figures S2 and S5). The addition of $CsPbBr_3$ enhances the growth of the PbS crystal domains leading to even narrower reflections (Figures S3 and S4 and Tables S3 and S4). This enhancement can be explained by the presence of $PbBr_2$, a phase with high solubility in PbS[67] and a large difference in melting point, which lowers the activation energy for diffusion.[68−70] Because no reflections associated with $PbBr_2$ are visible, we considered the possibility of other phases in the PbS−$PbBr_2$ phase diagram being formed. Still, $Pb_7S_2Br_{10}$, the only stable phase, was not observed in the diffraction patterns.[67] Recently, the metastable phase $Pb_4S_3Br_2$ was reported in NCs; this phase is not present in the XRD

https://dx.doi.org/10.1021/acsenergylett.0c02448
ACS Energy Lett. 2021, 6, 581−587

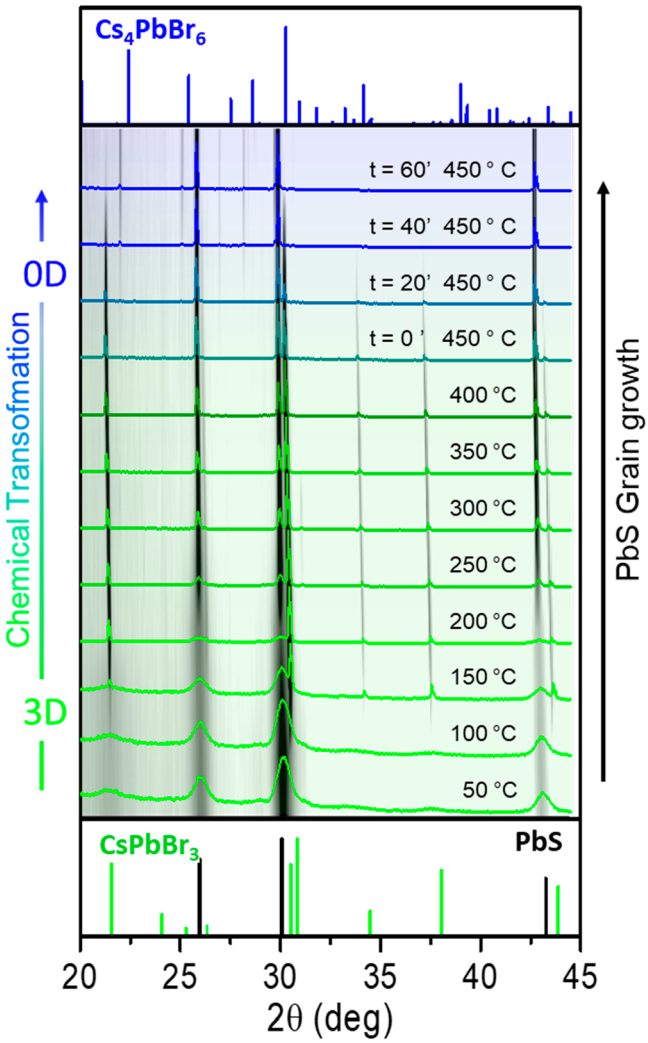

Figure 2. X-ray diffraction patterns of a mixture of PbS NCs and $CsPbBr_3$ NCs at different temperatures together with the reference patterns for the different crystal phases. In the 450 °C patterns, *t* indicates the time held at 450 °C before measurement. The patterns are overlapped with a 2D intensity plot to help to identify low intensity reflections (PbS PDF 00-002-0699, $CsPbBr_3$ PDF 00-054-0753, Cs_4PbBr_6 PDF 01-075-0412).

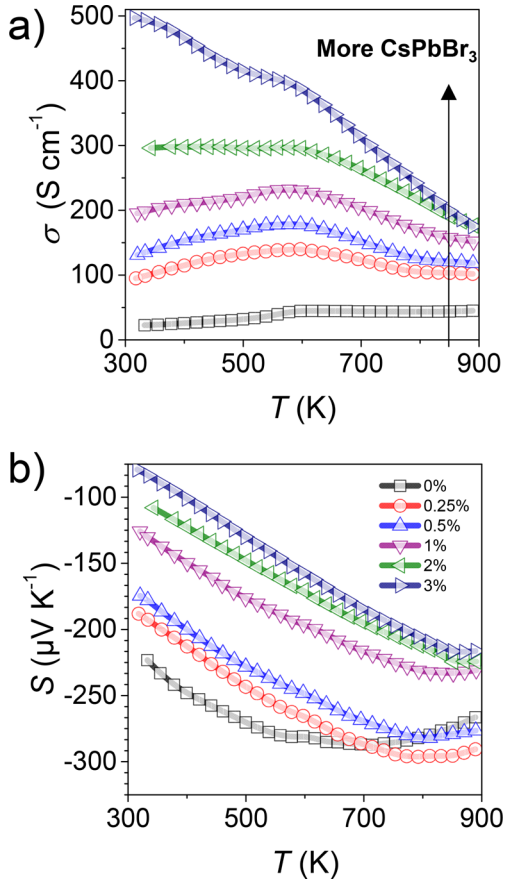

Figure 3. (a) Electrical conductivity and (b) Seebeck coefficient of the nanocomposites with increasing starting $CsPbBr_3$ concentration: 0% (black squares), 0.25% (red circles), 0.5% (blue triangles), 1% (purple triangles), 2% (green triangles), and 3% (dark blue triangles).

patterns, and we disregarded it because of the high temperature and long reaction time, which are not compatible with such a kinetically stabilized phase.[71] Previous studies showed pure $CsPbBr_3$ NCs undergo partial transformation to the lead-rich $CsPb_2Br_5$; this phase is not present in our experiments.[64] These observations suggest that bromide substitutes sulfide in PbS, doping the matrix as expressed in the chemical reactions in Scheme 1.

To test the doping efficiency, we prepared pellets with the proper nominal $CsPbBr_3$ concentrations to achieve charge carrier concentrations between 10^{19} and 10^{20} cm^{-3}, which is close to the optimal charge carrier concentration for thermoelectrics.[72,73] The molar amount of Br introduced is referred to the amount of S, *X*% = 0.25, 0.50, 1, 2, 3 (see the Supporting Information, page S1).

Panels a and b of Figure 3 show the electrical conductivity and Seebeck coefficient of the samples between room temperature and 900 K, respectively. At low temperatures, the absolute value of the Seebeck coefficient decreases and the electrical conductivity increases with the starting concentration of $CsPbBr_3$, proving the doping effect of the transformation (Supporting Information, page S8).[72] Besides, the negative sign of the Seebeck coefficient confirms the n-type character of the obtained nanocomposites. These results are consistent with the charge carrier concentrations measured by Hall effect (Table S2), which correspond exactly to one-half of the total Br concentration, as expected from the reaction in Scheme 1. The doping effect of $CsPbBr_3$ is independent of the use of NCs; ground perovskite crystals react with PbS in the same way. However, NCs provide a much shorter ion diffusion path and better mixing with PbS, which lead to faster kinetics (Supporting Information, page S10).

The observed tendencies in the electrical conductivity of nanostructured materials are a trade-off between many effects. On the one hand, the thermal excitation of carriers through energy barriers (grain boundaries) leads to an increase of the conductivity with temperature. This effect dominates at low temperatures in samples with smaller grains. On the other hand, an increase in temperature enhances charge carrier scattering. This is the typical behavior of heavily doped semiconductors and metals. Additionally, as the temperature increases, thermal excitation of minority carriers (bipolar effect) occurs. Consequently, the absolute value of the Seebeck coefficient starts decreasing. The higher the doping level, the higher the temperature at which this effect is perceptible.[61]

https://dx.doi.org/10.1021/acsenergylett.0c02448
ACS Energy Lett. 2021, 6, 581−587

The XRD patterns of the produced pellets show neither $CsPbBr_3$ nor Cs_4PbBr_6 reflections (Figure S6), which we associate with the low content of perovskite required for the doping level targeted. To demonstrate that the pelletized material contains Cs_4PbBr_6, we evaluated the microscopic structure of the bulk nanocomposites (Figure 4) by high-resolution transmission electron microscopy (HRTEM). A 0.5% pellet was thinned to electron transparency by Ar^+ polishing to produce a self-suspended lamella. Figure 4d shows an HRTEM micrograph obtained from a large PbS grain (defined as the matrix) containing multiple precipitates. The power spectrum of the highlighted area shows diffraction spots of the matrix and the precipitates, along with satellite spots of the Moiré fringes, which are formed because of orientation differences between the matrix and precipitates. Inverse Fourier (frequency) filtering of the power spectrum allowed mapping the matrix and the nanodomains. The matrix phase (in red) is identified as FCC PbS (space group $Fm\bar{3}m$) with a lattice parameter a = 0.5936 nm visualized along its [011] axis. The nanodomain (in green) corresponds to the same PbS phase visualized along the [001] zone axis. We performed the same analysis on the precipitate marked in Figure 4e. The diffraction spots observed in the power spectrum correspond to the matrix phase (in red) visualized along its [011] axis. The spots of the precipitate correspond to the hexagonal Cs_4PbBr_6 phase (space group $R\bar{3}c$:H) with lattice parameters a = 1.373 nm and c = 1.732 nm, which is visualized along the $[1\bar{1}02]$ zone axis. Because of the difficulty in analyzing all the precipitates crystallographically, to evaluate their nature we performed energy dispersion X-ray line scans across many precipitates. We found that they show no difference in composition with the matrix (Figure S7), proving that the vast majority of precipitates are PbS. The scans also show a small content of Br evenly distributed through the nanocomposites as expected in its role as a dopant. In short, HRTEM revealed that the doped samples are composed of a PbS matrix with a large amount of PbS nanodomains and randomly distributed Cs_4PbBr_6 nanoprecipitates (Figure 4), confirming the chemical transformation observed by XRD.

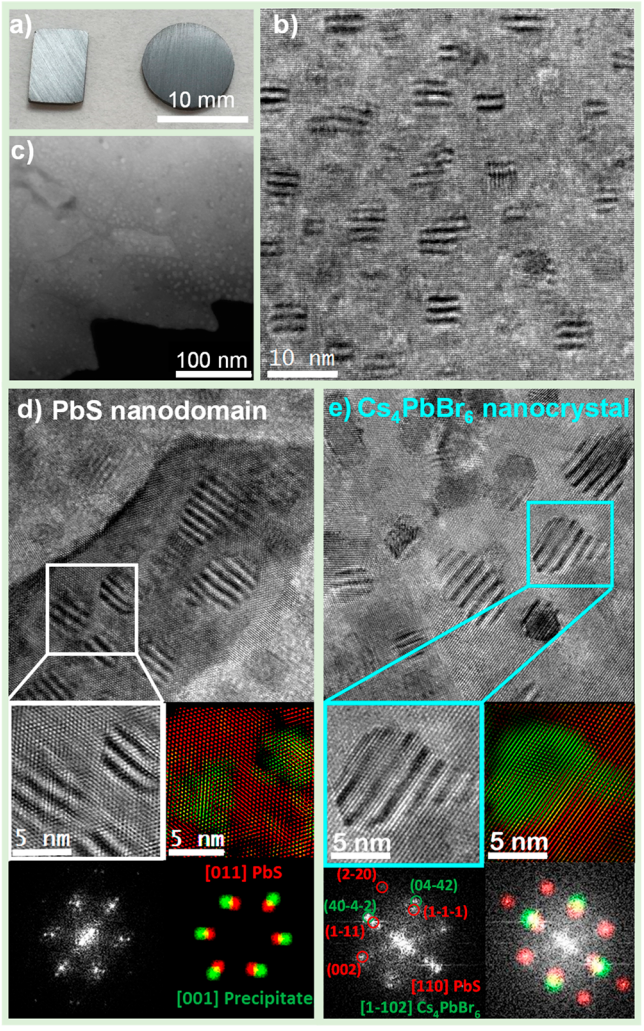

Figure 4. Structural analysis of a PbS−Cs_4PbBr_6 nanocomposite. The TEM sample is a self-suspended lamella prepared by Ar^+ ion milling. (a) Photograph of the pellets used to measure the electrical conductivity and the Seebeck coefficient; (b) HRTEM micrograph and (c) low-magnification high-angle annular dark field scanning transmission microscopy (HAADF-STEM) micrograph revealing the presence of small precipitates along the grains; (d) PbS nanodomains, detail of the white squared area and its corresponding power spectrum and structural maps of the PbS matrix (in red) and nanodomains (in green) along with the applied maps for inverse Fourier filtering; (e) detail of a Cs_4PbBr_6 nanoprecipitate and its corresponding power spectrum and structural maps of the PbS matrix (in red) and a Cs_4PbBr_6 precipitate (in green) are shown along with the applied maps for inverse Fourier filtering.

In summary, we showed that $CsPbBr_3$ and PbS react to give the lead depleted Cs_4PbBr_6 phase. The byproduct of the transformation, $PbBr_2$, dissolves in the PbS matrix, leading to doped nanocomposites and inducing grain growth while Cs_4PbBr_6 forms nanoprecipitates. We made use of this transformation to simultaneously dope and introduce a secondary phase in n-type PbS nanocomposites. These results validate this new doping strategy for nanocomposites based on NC blending that involves the reaction of one of the components. This approach is not limited to the preparation of bulk samples at high pressures but could also be applied to the preparation of films or other nanocomposites because the reaction that leads to doping is also demonstrated at ambient pressure. Finally, our results reassess the intrinsic instability of metal halide perovskites and are therefore of high relevance for applications where these materials are exposed to high energy densities.

■ ASSOCIATED CONTENT

Supporting Information

The Supporting Information is available free of charge at https://pubs.acs.org/doi/10.1021/acsenergylett.0c02448.

Chemicals, syntheses and preparation of the pellets. Details on the structural characterization and transport measurements (PDF)

■ AUTHOR INFORMATION

Corresponding Author

Maria Ibáñez − *Institute of Science and Technology Austria, Klosterneuburg 3400, Austria;* orcid.org/0000-0001-5013-2843; Email: mibanez@ist.ac.at

Authors

Mariano Calcabrini − *Institute of Science and Technology Austria, Klosterneuburg 3400, Austria*

https://dx.doi.org/10.1021/acsenergylett.0c02448
ACS Energy Lett. 2021, 6, 581−587

Aziz Genç − *Catalan Institute of Nanoscience and Nanotechnology (ICN2), CSIC and BIST, Campus UAB, Bellaterra, Barcelona 08193, Catalonia, Spain; Materials Science and Engineering Department, Izmir Institute of Technology, İzmir, Turkey*

Yu Liu − *Institute of Science and Technology Austria, Klosterneuburg 3400, Austria;* orcid.org/0000-0001-7313-6740

Tobias Kleinhanns − *Institute of Science and Technology Austria, Klosterneuburg 3400, Austria*

Seungho Lee − *Institute of Science and Technology Austria, Klosterneuburg 3400, Austria;* orcid.org/0000-0002-6962-8598

Dmitry N. Dirin − *Department of Chemistry and Applied Biosciences, ETH Zürich, Zurich CH-8093, Switzerland; Empa-Swiss Federal Laboratories for Materials Science and Technology, Zurich CH-8600, Switzerland;* orcid.org/0000-0002-5187-4555

Quinten A. Akkerman − *Department of Chemistry and Applied Biosciences, ETH Zürich, Zurich CH-8093, Switzerland; Empa-Swiss Federal Laboratories for Materials Science and Technology, Zurich CH-8600, Switzerland*

Maksym V. Kovalenko − *Department of Chemistry and Applied Biosciences, ETH Zürich, Zurich CH-8093, Switzerland; Empa-Swiss Federal Laboratories for Materials Science and Technology, Zurich CH-8600, Switzerland;* orcid.org/0000-0002-6396-8938

Jordi Arbiol − *Catalan Institute of Nanoscience and Nanotechnology (ICN2), CSIC and BIST, Campus UAB, Bellaterra, Barcelona 08193, Catalonia, Spain; ICREA, Barcelona 08010, Catalonia, Spain;* orcid.org/0000-0002-0695-1726

Complete contact information is available at: https://pubs.acs.org/10.1021/acsenergylett.0c02448

Notes

The authors declare no competing financial interest.

■ ACKNOWLEDGMENTS

M.C. has received funding from the European Union's Horizon 2020 research and innovation programme under the Marie Skłodowska-Curie Grant Agreement No. 665385. ICN2 acknowledges funding from Generalitat de Catalunya 2017 SGR 327. ICN2 is supported by the Severo Ochoa program from Spanish MINECO (Grant No. SEV-2017-0706) and is funded by the CERCA Programme/Generalitat de Catalunya. This project has received funding from the European Union's Horizon 2020 research and innovation programme under grant agreement No 823717 − ESTEEM3. M.V.K. acknowledges the support by the European Research Council under the Horizon 2020 Framework Program (ERC Consolidator Grant SCALE-HALO Grant Agreement No. 819740) and by FET-OPEN project no. 862656 (DROP-IT).

■ REFERENCES

(1) Shi, D.; Adinolfi, V.; Comin, R.; Yuan, M.; Alarousu, E.; Buin, A.; Chen, Y.; Hoogland, S.; Rothenberger, A.; Katsiev, K.; Losovyj, Y.; Zhang, X.; Dowben, P. A.; Mohammed, O. F.; Sargent, E. H.; Bakr, O. M. Low Trap-State Density and Long Carrier Diffusion in Organolead Trihalide Perovskite Single Crystals. *Science* **2015**, *347* (6221), 519−522.

(2) Maculan, G.; Sheikh, A. D.; Abdelhady, A. L.; Saidaminov, M. I.; Haque, M. A.; Murali, B.; Alarousu, E.; Mohammed, O. F.; Wu, T.; Bakr, O. M. $CH_3NH_3PbCl_3$ Single Crystals: Inverse Temperature Crystallization and Visible-Blind UV-Photodetector. *J. Phys. Chem. Lett.* **2015**, *6* (19), 3781−3786.

(3) Saidaminov, M. I.; Abdelhady, A. L.; Murali, B.; Alarousu, E.; Burlakov, V. M.; Peng, W.; Dursun, I.; Wang, L.; He, Y.; MacUlan, G.; Goriely, A.; Wu, T.; Mohammed, O. F.; Bakr, O. M. High-Quality Bulk Hybrid Perovskite Single Crystals within Minutes by Inverse Temperature Crystallization. *Nat. Commun.* **2015**, *6* (1), 7586.

(4) Manser, J. S.; Christians, J. A.; Kamat, P. V. Intriguing Optoelectronic Properties of Metal Halide Perovskites. *Chem. Rev.* **2016**, *116* (21), 12956−13008.

(5) Fang, H. H.; Adjokatse, S.; Wei, H.; Yang, J.; Blake, G. R.; Huang, J.; Even, J.; Loi, M. A. Ultrahigh Sensitivity of Methylammonium Lead Tribromide Perovskite Single Crystals to Environmental Gases. *Sci. Adv.* **2016**, *2* (7), e1600534.

(6) Sutton, R. J.; Eperon, G. E.; Miranda, L.; Parrott, E. S.; Kamino, B. A.; Patel, J. B.; Hörantner, M. T.; Johnston, M. B.; Haghighirad, A. A.; Moore, D. T.; Snaith, H. J. Bandgap-Tunable Cesium Lead Halide Perovskites with High Thermal Stability for Efficient Solar Cells. *Adv. Energy Mater.* **2016**, *6* (8), 1502458.

(7) McMeekin, D. P.; Sadoughi, G.; Rehman, W.; Eperon, G. E.; Saliba, M.; Hörantner, M. T.; Haghighirad, A.; Sakai, N.; Korte, L.; Rech, B.; Johnston, M. B.; Herz, L. M.; Snaith, H. J. A Mixed-Cation Lead Mixed-Halide Perovskite Absorber for Tandem Solar Cells. *Science* **2016**, *351* (6269), 151−155.

(8) Liu, X. K.; Xu, W.; Bai, S.; Jin, Y.; Wang, J.; Friend, R. H.; Gao, F. Metal Halide Perovskites for Light-Emitting Diodes. *Nat. Mater.* **2021**, *20*, 10−21.

(9) Noculak, A.; Noculak, A.; Morad, V.; Morad, V.; McCall, K. M.; Yakunin, S.; Shynkarenko, Y.; Yakunin, S.; Shynkarenko, Y.; Wörle, M.; Kovalenko, M. V. Bright Blue and Green Luminescence of Sb(III) in Double Perovskite Cs_2MInCl_6 (M = Na, K) Matrices. *Chem. Mater.* **2020**, *32* (12), 5118−5124.

(10) Jena, A. K.; Kulkarni, A.; Miyasaka, T. Halide Perovskite Photovoltaics: Background, Status, and Future Prospects. *Chem. Rev.* **2019**, *119* (5), 3036−3103.

(11) Brenner, P.; Bar-On, O.; Jakoby, M.; Allegro, I.; Richards, B. S.; Paetzold, U. W.; Howard, I. A.; Scheuer, J.; Lemmer, U. Continuous Wave Amplified Spontaneous Emission in Phase-Stable Lead Halide Perovskites. *Nat. Commun.* **2019**, *10* (1), 1−7.

(12) Akkerman, Q. A.; Rainò, G.; Kovalenko, M. V.; Manna, L. Genesis, Challenges and Opportunities for Colloidal Lead Halide Perovskite Nanocrystals. *Nat. Mater.* **2018**, *17* (5), 394−405.

(13) Bertolotti, F.; Protesescu, L.; Kovalenko, M. V.; Yakunin, S.; Cervellino, A.; Billinge, S. J. L.; Terban, M. W.; Pedersen, J. S.; Masciocchi, N.; Guagliardi, A. Coherent Nanotwins and Dynamic Disorder in Cesium Lead Halide Perovskite Nanocrystals. *ACS Nano* **2017**, *11* (4), 3819−3831.

(14) Aebli, M.; Benin, B. M.; McCall, K. M.; Morad, V.; Thöny, D.; Grützmacher, H.; Kovalenko, M. V. White $CsPbBr_3$: Characterizing the One-Dimensional Cesium Lead Bromide Polymorph. *Helv. Chim. Acta* **2020**, *103* (7), e2000080.

(15) Piveteau, L.; Aebli, M.; Yazdani, N.; Millen, M.; Korosec, L.; Krieg, F.; Benin, B. M.; Morad, V.; Piveteau, C.; Shiroka, T.; Comas-Vives, A.; Copéret, C.; Lindenberg, A. M.; Wood, V.; Verel, R.; Kovalenko, M. V. Bulk and Nanocrystalline Cesium Lead-Halide Perovskites as Seen by Halide Magnetic Resonance. *ACS Cent. Sci.* **2020**, *6* (7), 1138−1149.

(16) Yin, J.; Maity, P.; De Bastiani, M.; Dursun, I.; Bakr, O. M.; Brédas, J. L.; Mohammed, O. F. Molecular Behavior of Zero-Dimensional Perovskites. *Sci. Adv.* **2017**, *3* (12), e1701793.

(17) Akkerman, Q. A.; Manna, L. What Defines a Halide Perovskite? *ACS Energy Lett.* **2020**, *5* (2), 604−610.

(18) Kovalenko, M. V.; Protesescu, L.; Bodnarchuk, M. I. Properties and Potential Optoelectronic Applications of Lead Halide Perovskite Nanocrystals. *Science* **2017**, *358* (6364), 745−750.

(19) Li, Y.; Huang, H.; Xiong, Y.; Kershaw, S. V.; Rogach, A. L. Reversible Transformation between $CsPbBr_3$ and Cs_4PbBr_6 Nanocrystals. *CrystEngComm* **2018**, *20* (34), 4900−4904.

(20) Palazon, F.; Urso, C.; De Trizio, L.; Akkerman, Q.; Marras, S.; Locardi, F.; Nelli, I.; Ferretti, M.; Prato, M.; Manna, L. Postsynthesis Transformation of Insulating Cs_4PbBr_6 Nanocrystals into Bright Perovskite $CsPbBr_3$ through Physical and Chemical Extraction of CsBr. *ACS Energy Lett.* **2017**, *2* (10), 2445−2448.
(21) Wu, L.; Hu, H.; Xu, Y.; Jiang, S.; Chen, M.; Zhong, Q.; Yang, D.; Liu, Q.; Zhao, Y.; Sun, B.; Zhang, Q.; Yin, Y. From Nonluminescent Cs_4PbX_6 (X = Cl, Br, I) Nanocrystals to Highly Luminescent $CsPbX_3$ Nanocrystals: Water-Triggered Transformation through a CsX-Stripping Mechanism. *Nano Lett.* **2017**, *17* (9), 5799−5804.
(22) Palazon, F.; Almeida, G.; Akkerman, Q. A.; De Trizio, L.; Dang, Z.; Prato, M.; Manna, L. Changing the Dimensionality of Cesium Lead Bromide Nanocrystals by Reversible Postsynthesis Transformations with Amines. *Chem. Mater.* **2017**, *29* (10), 4167−4171.
(23) Liu, Z.; Bekenstein, Y.; Ye, X.; Nguyen, S. C.; Swabeck, J.; Zhang, D.; Lee, S. T.; Yang, P.; Ma, W.; Alivisatos, A. P. Ligand Mediated Transformation of Cesium Lead Bromide Perovskite Nanocrystals to Lead Depleted Cs_4PbBr_6 Nanocrystals. *J. Am. Chem. Soc.* **2017**, *139* (15), 5309−5312.
(24) Zhang, X.; Wu, X.; Liu, X.; Chen, G.; Wang, Y.; Bao, J.; Xu, X.; Liu, X.; Zhang, Q.; Yu, K.; Wei, W.; Liu, J.; Xu, J.; Jiang, H.; Wang, P.; Wang, X. Heterostructural $CsPbX_3$-PbS (X = Cl, Br, I) Quantum Dots with Tunable Vis-NIR Dual Emission. *J. Am. Chem. Soc.* **2020**, *142* (9), 4464−4471.
(25) Miranti, R.; Shin, D.; Septianto, R. D.; Ibáñez, M.; Kovalenko, M. V.; Matsushita, N.; Iwasa, Y.; Bisri, S. Z. Exclusive Electron Transport in Core@Shell PbTe@PbS Colloidal Semiconductor Nanocrystal Assemblies. *ACS Nano* **2020**, *14* (3), 3242−3250.
(26) Balazs, D. M.; Bijlsma, K. I.; Fang, H.-H. H.; Dirin, D. N.; Döbeli, M.; Kovalenko, M. V.; Loi, M. A. Stoichiometric Control of the Density of States in PbS Colloidal Quantum Dot Solids. *Sci. Adv.* **2017**, *3* (9), eaao1558.
(27) Gilmore, R. H.; Lee, E. M. Y.; Weidman, M. C.; Willard, A. P.; Tisdale, W. A. Charge Carrier Hopping Dynamics in Homogeneously Broadened PbS Quantum Dot Solids. *Nano Lett.* **2017**, *17* (2), 893−901.
(28) Shulga, A. G.; Kahmann, S.; Dirin, D. N.; Graf, A.; Zaumseil, J.; Kovalenko, M. V.; Loi, M. A. Electroluminescence Generation in PbS Quantum Dot Light-Emitting Field-Effect Transistors with Solid-State Gating. *ACS Nano* **2018**, *12* (12), 12805−12813.
(29) Speirs, M. J.; Balazs, D. M.; Dirin, D. N.; Kovalenko, M. V.; Loi, M. A. Increased Efficiency in Pn-Junction PbS QD Solar Cells via NaHS Treatment of the p-Type Layer. *Appl. Phys. Lett.* **2017**, *110* (10), 103904.
(30) Stavrinadis, A.; Pradhan, S.; Papagiorgis, P.; Itskos, G.; Konstantatos, G. Suppressing Deep Traps in PbS Colloidal Quantum Dots via Facile Iodide Substitutional Doping for Solar Cells with Efficiency > 10%. *ACS Energy Lett.* **2017**, *2* (4), 739−744.
(31) Wang, Y.; Liu, Z.; Huo, N.; Li, F.; Gu, M.; Ling, X.; Zhang, Y.; Lu, K.; Han, L.; Fang, H.; Shulga, A. G.; Xue, Y.; Zhou, S.; Yang, F.; Tang, X.; Zheng, J.; Antonietta Loi, M.; Konstantatos, G.; Ma, W. Room-Temperature Direct Synthesis of Semi-Conductive PbS Nanocrystal Inks for Optoelectronic Applications. *Nat. Commun.* **2019**, *10* (1), 5136.
(32) Nienhaus, L.; Wu, M.; Geva, N.; Shepherd, J. J.; Wilson, M. W. B.; Bulović, V.; Van Voorhis, T.; Baldo, M. A.; Bawendi, M. G. Speed Limit for Triplet-Exciton Transfer in Solid-State PbS Nanocrystal-Sensitized Photon Upconversion. *ACS Nano* **2017**, *11* (8), 7848.
(33) Saran, R.; Curry, R. J. Lead Sulphide Nanocrystal Photodetector Technologies. *Nat. Photonics* **2016**, *10* (2), 81−92.
(34) Tang, H.; Zhong, J.; Chen, W.; Shi, K.; Mei, G.; Zhang, Y.; Wen, Z.; Müller-Buschbaum, P.; Wu, D.; Wang, K.; Sun, X. W. Lead Sulfide Quantum Dot Photodetector with Enhanced Responsivity through a Two-Step Ligand-Exchange Method. *ACS Appl. Nano Mater.* **2019**, *2* (10), 6135−6143.
(35) Ibáñez, M.; Luo, Z.; Genç, A.; Piveteau, L.; Ortega, S.; Cadavid, D.; Dobrozhan, O.; Liu, Y.; Nachtegaal, M.; Zebarjadi, M.; Arbiol, J.; Kovalenko, M. V.; Cabot, A. High-Performance Thermoelectric Nanocomposites from Nanocrystal Building Blocks. *Nat. Commun.* **2016**, *7* (1), 10766.
(36) Ibáñez, M.; Korkosz, R. J.; Luo, Z.; Riba, P.; Cadavid, D.; Ortega, S.; Cabot, A.; Kanatzidis, M. G. Electron Doping in Bottom-up Engineered Thermoelectric Nanomaterials through HCl-Mediated Ligand Displacement. *J. Am. Chem. Soc.* **2015**, *137* (12), 4046−4049.
(37) Xu, B.; Feng, T.; Li, Z.; Pantelides, S. T.; Wu, Y. Constructing Highly Porous Thermoelectric Monoliths with High-Performance and Improved Portability from Solution-Synthesized Shape-Controlled Nanocrystals. *Nano Lett.* **2018**, *18* (6), 4034−4039.
(38) Ibáñez, M.; Hasler, R.; Liu, Y.; Dobrozhan, O.; Nazarenko, O.; Cadavid, D.; Cabot, A.; Kovalenko, M. V. Tuning P-Type Transport in Bottom-Up-Engineered Nanocrystalline Pb Chalcogenides Using Alkali Metal Chalcogenides as Capping Ligands. *Chem. Mater.* **2017**, *29* (17), 7093−7097.
(39) Dalpian, G. M.; Chelikowsky, J. R. Self-Purification in Semiconductor Nanocrystals. *Phys. Rev. Lett.* **2006**, *96* (22), 226802.
(40) Norris, D. J.; Efros, A. L.; Erwin, S. C. Doped Nanocrystals. *Science* **2008**, *319* (5871), 1776−1779.
(41) Oh, S. J.; Berry, N. E.; Choi, J.-H. H.; Gaulding, E. A.; Paik, T.; Hong, S.-H. H.; Murray, C. B.; Kagan, C. R. Stoichiometric Control of Lead Chalcogenide Nanocrystal Solids to Enhance Their Electronic and Optoelectronic Device Performance. *ACS Nano* **2013**, *7* (3), 2413−2421.
(42) Buonsanti, R.; Milliron, D. J. Chemistry of Doped Colloidal Nanocrystals. *Chem. Mater.* **2013**, *25* (8), 1305−1317.
(43) Du, M. H.; Erwin, S. C.; Efros, A. L. Trapped-Dopant Model of Doping in Semiconductor Nanocrystals. *Nano Lett.* **2008**, *8* (9), 2878−2882.
(44) Yazdani, N.; Andermatt, S.; Yarema, M.; Farto, V.; Bani-Hashemian, M. H.; Volk, S.; Lin, W. M. M.; Yarema, O.; Luisier, M.; Wood, V. Charge Transport in Semiconductors Assembled from Nanocrystal Quantum Dots. *Nat. Commun.* **2020**, *11* (1), 2852.
(45) Ning, Z.; Voznyy, O.; Pan, J.; Hoogland, S.; Adinolfi, V.; Xu, J.; Li, M.; Kirmani, A. R.; Sun, J. P.; Minor, J.; Kemp, K. W.; Dong, H.; Rollny, L.; Labelle, A.; Carey, G.; Sutherland, B.; Hill, I.; Amassian, A.; Liu, H.; Tang, J.; Bakr, O. M.; Sargent, E. H. Air-Stable n-Type Colloidal Quantum Dot Solids. *Nat. Mater.* **2014**, *13* (8), 822−828.
(46) Nugraha, M. I.; Kumagai, S.; Watanabe, S.; Sytnyk, M.; Heiss, W.; Loi, M. A.; Takeya, J. Enabling Ambipolar to Heavy N-Type Transport in PbS Quantum Dot Solids through Doping with Organic Molecules. *ACS Appl. Mater. Interfaces* **2017**, *9* (21), 18039−18045.
(47) Robin, A.; Livache, C.; Ithurria, S.; Lacaze, E.; Dubertret, B.; Lhuillier, E. Surface Control of Doping in Self-Doped Nanocrystals. *ACS Appl. Mater. Interfaces* **2016**, *8* (40), 27122−27128.
(48) Choi, M. J.; García de Arquer, F. P.; Proppe, A. H.; Seifitokaldani, A.; Choi, J.; Kim, J.; Baek, S. W.; Liu, M.; Sun, B.; Biondi, M.; Scheffel, B.; Walters, G.; Nam, D. H.; Jo, J. W.; Ouellette, O.; Voznyy, O.; Hoogland, S.; Kelley, S. O.; Jung, Y. S.; Sargent, E. H. Cascade Surface Modification of Colloidal Quantum Dot Inks Enables Efficient Bulk Homojunction Photovoltaics. *Nat. Commun.* **2020**, *11* (1), 103.
(49) Wang, H.; Butler, D. J.; Straus, D. B.; Oh, N.; Wu, F.; Guo, J.; Xue, K.; Lee, J. D.; Murray, C. B.; Kagan, C. R. Air-Stable $CuInSe_2$ Nanocrystal Transistors and Circuits via Post-Deposition Cation Exchange. *ACS Nano* **2019**, *13* (2), 2324−2333.
(50) Chakraborty, P.; Jin, Y.; Barrows, C. J.; Dunham, S. T.; Gamelin, D. R. Kinetics of Isovalent (Cd^{2+}) and Aliovalent (In^{3+}) Cation Exchange in $Cd_{1-x}Mn_xSe$ Nanocrystals. *J. Am. Chem. Soc.* **2016**, *138* (39), 12885−12893.
(51) Liu, Y.; Cadavid, D.; Ibáñez, M.; Ortega, S.; Martí-Sánchez, S.; Dobrozhan, O.; Kovalenko, M. V.; Arbiol, J.; Cabot, A. Thermoelectric Properties of Semiconductor-Metal Composites Produced by Particle Blending. *APL Mater.* **2016**, *4* (10), 104813.
(52) Urban, J. J.; Talapin, D. V.; Shevchenko, E. V.; Kagan, C. R.; Murray, C. B. Synergism in Binary Nanocrystal Superlattices Leads to Enhanced P-Type Conductivity in Self-Assembled PbTe/Ag_2Te Thin Films. *Nat. Mater.* **2007**, *6* (2), 115−121.

https://dx.doi.org/10.1021/acsenergylett.0c02448
ACS Energy Lett. 2021, 6, 581−587

(53) Zhao, D.; Huang, J.; Qin, R.; Yang, G.; Yu, J. Perovskite Photodetectors: Efficient Visible−Near-Infrared Hybrid Perovskite:PbS Quantum Dot Photodetectors Fabricated Using an Antisolvent Additive Solution Process. *Adv. Opt. Mater.* **2018**, *6* (23), 1870090.
(54) Liu, C.; Peng, H.; Wang, K.; Wei, C.; Wang, Z.; Gong, X. PbS Quantum Dots-Induced Trap-Assisted Charge Injection in Perovskite Photodetectors. *Nano Energy* **2016**, *30*, 27−35.
(55) Piatkowski, P.; Masi, S.; Galar, P.; Gutiérrez, M.; Ngo, T. T.; Mora-Seró, I.; Douhal, A. Deciphering the Role of Quantum Dot Size in the Ultrafast Charge Carrier Dynamics at the Perovskite-Quantum Dot Interface. *J. Mater. Chem. C* **2020**, *8* (42), 14834−14844.
(56) Gong, X.; Yang, Z.; Walters, G.; Comin, R.; Ning, Z.; Beauregard, E.; Adinolfi, V.; Voznyy, O.; Sargent, E. H. Highly Efficient Quantum Dot Near-Infrared Light-Emitting Diodes. *Nat. Photonics* **2016**, *10* (4), 253−257.
(57) Ning, Z.; Gong, X.; Comin, R.; Walters, G.; Fan, F.; Voznyy, O.; Yassitepe, E.; Buin, A.; Hoogland, S.; Sargent, E. H. Quantum-Dot-in-Perovskite Solids. *Nature* **2015**, *523* (7560), 324−328.
(58) Yang, Z.; Janmohamed, A.; Lan, X.; García De Arquer, F. P.; Voznyy, O.; Yassitepe, E.; Kim, G.-H.; Ning, Z.; Gong, X.; Comin, R.; Sargent, E. H. Colloidal Quantum Dot Photovoltaics Enhanced by Perovskite Shelling. *Nano Lett.* **2015**, *15*, 7539.
(59) Liu, M.; Chen, Y.; Tan, C. S.; Quintero-Bermudez, R.; Proppe, A. H.; Munir, R.; Tan, H.; Voznyy, O.; Scheffel, B.; Walters, G.; Kam, A. P. T.; Sun, B.; Choi, M. J.; Hoogland, S.; Amassian, A.; Kelley, S. O.; García de Arquer, F. P.; Sargent, E. H. Lattice Anchoring Stabilizes Solution-Processed Semiconductors. *Nature* **2019**, *570* (7759), 96−101.
(60) Sytnyk, M.; Yakunin, S.; Schöfberger, W.; Lechner, R. T.; Burian, M.; Ludescher, L.; Killilea, N. A.; Yousefiamin, A.; Kriegner, D.; Stangl, J.; Groiss, H.; Heiss, W. Quasi-Epitaxial Metal-Halide Perovskite Ligand Shells on PbS Nanocrystals. *ACS Nano* **2017**, *11* (2), 1246−1256.
(61) Wang, H.; Schechtel, E.; Pei, Y.; Snyder, G. J. High Thermoelectric Effinciency of N-Type PbS. *Adv. Energy Mater.* **2013**, *3* (4), 488−495.
(62) Zhang, Q.; Wang, B.; Zheng, W.; Kong, L.; Wan, Q.; Zhang, C.; Li, Z.; Cao, X.; Liu, M.; Li, L. Ceramic-like Stable $CsPbBr_3$ Nanocrystals Encapsulated in Silica Derived from Molecular Sieve Templates. *Nat. Commun.* **2020**, *11* (1), 31.
(63) Palazon, F.; Di Stasio, F.; Lauciello, S.; Krahne, R.; Prato, M.; Manna, L. Evolution of $CsPbBr_3$ Nanocrystals upon Post-Synthesis Annealing under an Inert Atmosphere. *J. Mater. Chem. C* **2016**, *4* (39), 9179−9182.
(64) Palazon, F.; Dogan, S.; Marras, S.; Locardi, F.; Nelli, I.; Rastogi, P.; Ferretti, M.; Prato, M.; Krahne, R.; Manna, L. From $CsPbBr_3$ Nano-Inks to Sintered $CsPbBr_3$-$CsPb_2Br_5$ Films via Thermal Annealing: Implications on Optoelectronic Properties. *J. Phys. Chem. C* **2017**, *121* (21), 11956−11961.
(65) Tang, J.; Kemp, K. W.; Hoogland, S.; Jeong, K. S.; Liu, H.; Levina, L.; Furukawa, M.; Wang, X.; Debnath, R.; Cha, D.; Chou, K. W.; Fischer, A.; Amassian, A.; Asbury, J. B.; Sargent, E. H. Colloidal-Quantum-Dot Photovoltaics Using Atomic-Ligand Passivation. *Nat. Mater.* **2011**, *10* (10), 765−771.
(66) Tang, J.; Brzozowski, L.; Barkhouse, D. A. R.; Wang, X.; Debnath, R.; Wolowiec, R.; Palmiano, E.; Levina, L.; Pattantyus-Abraham, A. G.; Jamakosmanovic, D.; Sargent, E. H. Quantum Dot Photovoltaics in the Extreme Quantum Confinement Regime: The Surface-Chemical Origins of Exceptional Air- and Light-Stability. *ACS Nano* **2010**, *4* (2), 869−878.
(67) Rabenau, A.; Rau, H. Über Sulfidhalogenide Des Bleis Und Das Pb_4SeBr_6. *Z. Anorg. Allg. Chem.* **1969**, *369* (3−6), 295−305.
(68) German, R. M.; Rabin, B. H. Enhanced Sintering through Second Phase Additions. *Powder Metall.* **1985**, *28* (1), 7−12.
(69) Zovas, P. E.; German, R. M.; Hwang, K. S.; Li, C. J. Activated and Liquid-Phase Sintering—Progress and Problems. *J. Met.* **1983**, *35* (1), 28−33.
(70) Zhang, H.; Dasbiswas, K.; Ludwig, N. B.; Han, G.; Lee, B.; Vaikuntanathan, S.; Talapin, D. V. Stable Colloids in Molten Inorganic Salts. *Nature* **2017**, *542* (7641), 328−331.
(71) Toso, S.; Akkerman, Q. A.; Martín-García, B.; Prato, M.; Zito, J.; Infante, I.; Dang, Z.; Moliterni, A.; Giannini, C.; Bladt, E.; Lobato, I.; Ramade, J.; Bals, S.; Buha, J.; Spirito, D.; Mugnaioli, E.; Gemmi, M.; Manna, L. Nanocrystals of Lead Chalcohalides: A Series of Kinetically Trapped Metastable Nanostructures. *J. Am. Chem. Soc.* **2020**, *142* (22), 10198−10211.
(72) Snyder, G. J.; Toberer, E. S. Complex Thermoelectric Materials. *Nat. Mater.* **2008**, *7* (2), 105−114.
(73) Ortega, S.; Ibáñez, M.; Liu, Y.; Zhang, Y.; Kovalenko, M. V.; Cadavid, D.; Cabot, A. Bottom-up Engineering of Thermoelectric Nanomaterials and Devices from Solution-Processed Nanoparticle Building Blocks. *Chem. Soc. Rev.* **2017**, *46* (12), 3510−3528.

https://dx.doi.org/10.1021/acsenergylett.0c02448
ACS Energy Lett. 2021, 6, 581−587